Available online at www.sciencedirect.com
ScienceDirect
Journal of Sound and Vibration 302 (2007) 260–286
JOURNAL OF SOUND AND VIBRATION
www.elsevier.com/locate/jsvi

An analytical–numerical method to analyze single degree of freedom models under airblast loading

Manuel Campidelli[a], Erasmo Viola[b,*]

[a]Dipartimento di Strutture, Università della Calabria, Via P. Bucci, Cubo 39C, 87030 Rende (CS), Italia
[b]Dipartimento di Ingegneria delle Strutture, dei Trasporti, delle Acque, del Rilevamento, del Territorio (DISTART), Università degli Studi di Bologna, Viale Risorgimento 2, 40136 Bologna, Italia

Received 21 July 2006; received in revised form 7 November 2006; accepted 27 November 2006
Available online 24 January 2007

Abstract

In this paper, an analytical–numerical method to predict the response of a linear spring–mass system without damper, excited by a family of pulse loads, is proposed. The external loading is described by a four parameter expression, involving the peak overpressure, the loading duration and two parameters which characterize the pulse shape (λ and γ). A parametric analysis for ranges of pulse shape parameters suitable to describe a wavefront pressure profile produced by an airblast from high explosives is developed. The influence of the pulse shape on the dynamic load factor representation of structural response and on pressure–impulse isodamage curves is graphically shown. An expression of the transient response spectrum generated by a typical exponentially decaying load ($\lambda = 1$, $\gamma = 2.8$) is proposed, and a discussion about the formulation of a general expression for the transient response spectrum is introduced. Various features of the spectrum and pressure–impulse diagrams are analyzed, and all the problems concerning the building of graphics are discussed. Finally, a review of existing simplified isodamage curves is reported and an existing method to eliminate pulse shape effects, the effective pressure–impulse diagram, is discussed.

1. Introduction

Blast load effects from high explosives on structures involve a wide range of problems and often different methods of analysis, basically different from those given by other dynamic loads. For example, for pulse loads the maximum transient response is of primary importance.

The pressure load profile given by explosions can be considered either deterministic or aleatory. Although uncertainties concerning an explosion make a random model more appropriate, deterministic loadings are still useful to compare results of different models and to get a rapid assessment of structural behaviors. Baker et al. [1] suggested two different deterministic pressure profiles if a detonation or a deflagration occurs. Detonating explosives are characterized by loads with a step rise followed by an exponential decay. When deflagration occurs, the pressure profile suggested by Baker has a finite rise time, and the typical monotonic behavior of

*Corresponding author. Present address: DISTART, Università degli Studi di Bologna, Viale Risorgimento 2, 40136 Bologna, Italia. Tel.: +39 051 209 3510; fax: +39 051 209 3495.
E-mail address: erasmo.viola@mail.ing.unibo.it (E. Viola).

0022-460X/$ - see front matter © 2006 Published by Elsevier Ltd.
doi:10.1016/j.jsv.2006.11.024

Nomenclature

a_r, b_r	rth coefficients of the spectrum regression function
D	centroid distance of the pressure profile from the axis origin
DLF	dynamic load factor
DLF_f	dynamic load factor related to forced vibrations
DLF_l	dynamic load factor related to free vibrations
$DLF_{max}(\tau_d)$	response spectrum
$DLF_{max,1}$, $DLF_{max,2}$	relative maximum points of dynamic load factor
$f(\xi)$	normalized loading function with respect to the peak load value
f_1, f_2	functions of pulse shape parameters λ and γ
$F(t)$	loading function
F_{max}	peak value of loading function
g	degree of regression polynomial
$G(p, i)$	damage function
i	dimensionless impulse
i_A	dimensionless impulse corresponding to the inferior response limit
i_B	dimensionless impulse corresponding to the superior response limit
i_e	effective impulse
I	impulse
k	spring constant
m	lumped mass
m_1, m_2	parameters of regression p–i curves
n, n_0, n_1, n_2, n_3, n_4	arbitrary natural numbers
p	dimensionless pressure (or force)
p_A	dimensionless pressure corresponding to the inferior response limit
p_B	dimensionless pressure corresponding to the superior response limit
p_e	effective pressure
Q^2	sum of squared residuals
$S(\tau_d)$	response spectrum
S_r	hyperbolic function
t	time
t_d	positive phase duration (loading duration)
t_{max}	time corresponding to a maximum relative displacement
T	natural period of vibration
T	kinetic energy
w_j	weight of the jth point on p–i curves
W_e	work done by the external loading
X, Y	auxiliary variables
$y(t)$	mass displacement
$\dot{y}(t)$	mass speed
y_c	critical displacement
$y_f(t)$	mass displacement during forced vibration
$y_l(t)$	mass displacement during free vibration
y_{max}	maximum displacement (system response)
y_{st}	static displacement
$\beta_{i,1}$	ith coefficient of the regression function $m_1(D)$
$\beta_{i,2}$	ith coefficient of the regression function $m_2(D)$
β_{i,i_B}	ith coefficient of the regression function $i_B(D)$
β_{i,p_A}	ith coefficient of the regression function $p_A(D)$
β_{i,τ_1}	ith coefficient of the regression function $\tau_1(D)$
β_{i,τ_2}	ith coefficient of the regression function $\tau_2(D)$
ε	relative accuracy
γ	second pulse shape parameter
η_j	jth residual
Φ	elastic strain energy
λ	first pulse shape parameter
v	exponent in w_j expression
ϑ	inverse of dimensionless loading time
τ	dimensionless time
τ_1	inferior limit of response
τ_2	superior limit of response
τ_d	dimensionless loading duration
$\tau_{d,0}$	transition point abscissa of the response spectrum
τ_{max}	dimensionless time corresponding to a relative maximum displacement
ω	natural circular frequency of vibration
ξ	scaled time
ξ_0	centroid abscissa of scaled pressure profile
ψ	function of shape the parameters λ and γ
ζ_0	centroid ordinate of scaled pressure profile

pressure–impulse curves is not confirmed. Li and Meng [2,3] considered a general descending pulse load described by a four parameter expression involving the peak overpressure, the loading duration (or the positive phase duration of the blast wave if the negative one is neglected) and two shape parameters which characterize the load shape.

A random excitation of space structures was considered by Chang [4], who analyzed a free–free beam with a lumped mass and hysteretically damped; the cross spectral density function of the applied load was a Gaussian stochastic process in time. It was shown that larger uncertainties of random loads decrease the system reliability.

As far as the prediction of the structural behavior is concerned, another important topic is the choice of a versatile modeling scheme or approximate technique to rapidly assess structural response for a wide range of geometries. One of the most recent schemes was proposed by Schleyer and Hsu [5] for a class of problems in which elastic effects are significant, the pulse shape is irregular and boundary conditions are varying. On the other hand a simple single degree of freedom model (sdof model), although approximate, had been widely employed to predict the structural response of actual structures under blast loads [6–8]. For complex structures, Abrahamson and Lindberg [9] proposed to construct a critical pressure–impulse curve as the envelope of the critical load curves for the structural elements, schematized as sdof models.

It is well known that a sdof model can provide information just for one point in the structural system under consideration. A sdof model is useful for supporting the structural design because it allows to predict the overall response of a structure. However, it is limited for identifying more complex structural behavior. In general, structural models like plates and shells are more representative of the structural behavior and of the state of damage. Therefore, a sdof model can be regarded just as a first-order design method or a first step numerical method, useful when a structure is analyzed starting from simple numerical approaches, as noted by Krauthammer [8].

In this first-order method, the damping has been neglected. Indeed, although all dynamic systems contain damping to some degree, in case of structures with a load-time function described in Eq. (1) the damping effect is not significant if some conditions suggested by Biggs [10] are respected: the load duration must be short, as shown in Section 2.3, and the only output datum of interest is the maximum dynamic response of the structure.

Pulse shape effects on the structural response were considered by Youngdahl [11], who examined several kinds of structures with a rigid-plastic stress–strain relation (circular plate, reinforced circular cylindrical shell, free–free beam, circular shell with a ring load), under different load shapes (rectangular, linearly decaying, exponentially decaying, triangular and sinusoidal). He tried to eliminate the dependence of the response from the load shape by introducing two key parameters, the total impulse and the effective load, involving a loading function and two time parameters referring to the beginning and the end of the plastic deformation. A theoretical foundation for Youngdahl's work [11] was given by Li and Meng [3] for a rigid-plastic sdof model. In successive works Youngdahl [12,13] considered problems where P becomes a function both of position and time, or the stress–strain relation is more complex, such as the strain hardening. In this cases the calculation of effective parameters results more complicated. Abrahamson and Lindberg [9] suggested the use of a simple hyperbolic shape for the pressure–impulse diagram, which provided significant discrepancies (20–40%) with respect to the isodamage curves given by an exponentially and a linearly decaying load acting on a sdof model. Zhu et al. [14] used Youngdahl's work to develop simple characteristic curves for rigid-plastic structural models, as was done by Abrahamson and Lindberg.

Transverse shear effects on fully clamped circular plates, 'short' cylindrical shell and fully clamped beams were considered by Li and Jones [15–17], who established key parameters to decide when shear effects have to be taken into account.

The counterintuitive behavior of highly parametric sensitive systems loaded by detonations of low magnitude was observed for the first time by Symonds and Yu [18] for a pin-ended beam subjected to an uniformly distributed pressure load, with an elastic–plastic stress–strain relation. This problem, characterized by high sensitivity to the loading model and uncertain response, was also studied by Li and Liu [19] using a probabilistic method.

The aim of this paper is to generalize the work done by Li and Meng [2] for various load shapes, when elastic effects are significant. In fact, it has been demonstrated that elastic effects cannot be disregarded when

the ratio of initial kinetic energy to maximum elastic strain energy is larger than 10. When the structure is relatively stiff or the load duration is relatively long, the rigid plastic solution is non-conservative compared with the elastic–plastic solution. Therefore, in this paper the influence of the pulse shape on the dynamic load factor and pressure–impulse diagram is shown for a linear sdof model excited by a four parameter load function suitable to describe a monotonically descending pulse load. The knowledge of the transient response depending on the shape parameters is primarily important to understand the behavior of a sdof model with different stress–strain relations, which could be often simplified as broken lines. In the following analysis many problems concerning the response spectrum are highlighted, like the position of the spectrum transition point. A discussion about the formulation of a general expression for the transient response spectrum is reported. An analytical expression of isodamage curves is examined for different pulse shapes, and the validity of an effective pressure–impulse diagram proposed in Ref. [2] is discussed.

2. Response analysis

When a system configuration can be described by the displacement of a single point, the known principles of structural dynamics allow to convert the actual structures into a sdof model by using equivalent mass, damping and resistance function.

The pressure profile assumed by Li and Meng [2] for an explosive charge, is a generalized form of the Friedlander equation [20]:

$$F(t)=\begin{cases} F_{\max}\left(1-\lambda\dfrac{t}{t_d}\right)\exp\left(-\gamma\dfrac{t}{t_d}\right) & \text{for } 0\leqslant t\leqslant t_d,\\ 0 & \text{for } t>t_d, \end{cases} \tag{1}$$

where t is the time in seconds; $F_{\max}$ is the peak load value, in kN (if the load is a force) or in kN/m^2 (if it is a pressure); λ and γ are shape parameters; t_d is the duration of the loading positive phase. Since the negative phase can be neglected to evaluate the effect of an explosion, t_d represent the total duration of loading.

The load described from Eq. (1) acts on the structure with an impulse as follows:

$$I=\int_0^{t_d}F(t)\,\mathrm{d}t=F_{\max}t_d\psi(\lambda,\gamma),\quad \psi(\lambda,\gamma)=\frac{(\gamma-\lambda)(1-e^{-\gamma})+\lambda\gamma e^{-\gamma}}{\gamma^2}. \tag{2}$$

The effects on a linear spring–mass system loaded by a pulse load with $\lambda\in[0,1]$ and $\gamma\in[0,10]$ have been studied; these ranges are suitable to describe a pulse load from detonations that are characterized by a step rise and a following decay, with a fixed magnitude at $t=t_d$.

By applying D'Alembert's principle, the motion equation results:

$$m\ddot{y}+ky=F(t),\quad 0\leqslant t\leqslant t_d\quad\text{(forced vibrations)}, \tag{3a}$$

$$m\ddot{y}+ky=0,\quad t>t_d\quad\text{(free vibrations)}, \tag{3b}$$

with initial conditions:

$$i.c.\begin{cases} y(t=0)=0,\\ \dot{y}(t=0)=0, \end{cases} \tag{4}$$

where m and k are, respectively, the equivalent mass and stiffness and y is the mass displacement. To represent the system response, the following symbols are adopted:

$\omega=\sqrt{k/m}$ is the natural frequency of the structure;
$\tau=\omega t$ is the dimensionless time variable;
$\tau_d=\omega t_d$ is the dimensionless loading duration;
$t_{\max}$ is a point in the time domain corresponding to a relative maximum point of the displacement function;
$\tau_{\max}=\omega t_{\max}$ is a dimensionless time value corresponding to a relative maximum displacement;
$y_{\mathrm{st}}=F_{\max}/k$ is the static displacement;

$y_f(t)$ represents the displacement function for forced vibrations;
$y_l(t)$ is the displacement function for free vibrations;
$\mathrm{DLF}_f(\tau) = y_f/y_{\mathrm{st}}$ is the dynamic load factor of forced vibrations;
$\mathrm{DLF}_l(\tau) = y_l/y_{\mathrm{st}}$ is the dynamic load factor of free vibrations.

In order to calculate the solution of the motion equation during the forced vibrations, the general integral of the Eq. (3a) can be established by solving the Duhamel's integral applied to the assigned force. According to Biggs [10], we have

$$y_f(t) = \int_0^t \frac{F(t')}{\sqrt{mk}} \sin\left(\frac{t-t'}{\sqrt{m/k}}\right) \mathrm{d}t' = \frac{F_{\max}}{\sqrt{mk}} \int_0^t f(t') \sin\omega(t-t')\,\mathrm{d}t',$$

where $f(t')$ represents the load function from Eq. (1) normalized with respect to the peak value $F_{\max}$.

By defining

$$f_1(\lambda,\gamma,t_d) = 1 - \frac{2\lambda\gamma}{\gamma^2 + (\omega t_d)^2}, \quad f_2(\lambda,\gamma,t_d) = \lambda + \gamma f_1(\lambda,\gamma,t_d) \tag{5}$$

we get:

$$\mathrm{DLF}_f(\tau) = \frac{\tau_d^2}{\gamma^2+\tau_d^2}\left\{ f_2 \frac{\sin\tau}{\tau_d} - f_1\cos\tau + \left(f_1 - \lambda\frac{\tau}{\tau_d}\right)\exp\left(-\gamma\frac{\tau}{\tau_d}\right)\right\}. \tag{6}$$

From Eqs. (3b) and (6), the solution of the motion equation during the free vibrations can be obtained by imposing the continuity of the dynamic load factor and its first derivative at $\tau = \tau_d$:

$$\begin{cases} \mathrm{DLF}_l(\tau) = \dfrac{y_l(\tau)}{y_{\mathrm{st}}} = \mathrm{A}\cos\tau + \mathrm{B}\sin\tau, \\ \mathrm{A} = \dfrac{\tau_d^2}{\gamma^2+\tau_d^2}\left\{ -f_1 + e^{-\gamma}\left[(f_1-\lambda)\cos\tau_d + \dfrac{f_2-\lambda\gamma}{\tau_d}\sin\tau_d\right]\right\}, \\ \mathrm{B} = \dfrac{\tau_d^2}{\gamma^2+\tau_d^2}\left\{ \dfrac{f_2}{\tau_d} + e^{-\gamma}\left[(f_1-\lambda)\sin\tau_d - \dfrac{f_2-\lambda\gamma}{\tau_d}\cos\tau_d\right]\right\}. \end{cases} \tag{7}$$

2.1. Stationary points of the displacement function

During the free vibration phase, the time values when a relative maximum displacement is reached are established as follows:

$$\tau_{\max} = n\pi + \arctan\left(\frac{\mathrm{B}}{\mathrm{A}}\right), \quad n \in \mathbb{N}. \tag{8}$$

During the forced vibration phase, $\tau_{\max}$ is defined by equating to zero the first derivative of the displacement function which describes the forced vibrations:

$$\frac{\mathrm{d}y_f}{\mathrm{d}t}(t_{\max}) = \frac{\mathrm{d}}{\mathrm{d}t}\left\{ f_2\frac{\sin\omega t}{\omega t_d} - f_1\cos\omega t + \left(f_1 - \lambda\frac{t}{t_d}\right)\exp\left(-\gamma\frac{t}{t_d}\right)\right\}\Bigg|_{t=t_{\max}} = 0.$$

By defining a new variable $\vartheta = 1/\tau_d$, we obtain:

$$\varphi(\vartheta,\tau_{\max}) = f_1\sin\tau_{\max} + f_2\vartheta\cos\tau_{\max} - [f_2 - \lambda\gamma\vartheta\tau_{\max}]\exp(-\gamma\vartheta\tau_{\max}) = 0. \tag{9}$$

Eq. (9) represents an implicit function $\tau_{\max}(\vartheta)$, which can be simply calculated when $\vartheta \to 0$ (or $\tau_d \to +\infty$); in fact, from Eq. (1) we have:

$$\lim_{\tau_d\to+\infty} F(\tau) = \lim_{\tau_d\to+\infty} F_{\max}\left(1-\lambda\frac{\tau}{\tau_d}\right)\exp\left(-\gamma\frac{\tau}{\tau_d}\right) = F_{\max}. \tag{10}$$

When $\tau_d \to \infty$, Eq. (10) shows that the system is excited by a rectangular load (step rise, constant magnitude, step decay) with infinite duration for all the finite values of λ and γ. Therefore, the time values when a relative maximum displacement is reached can be deduced using the corresponding solution coming from a spring–mass system under a rectangular pressure profile:

$$\tau_{\max}(\tau_d \to +\infty) = \tau_{\max}(\vartheta \to 0) = n\pi, \quad n \in \mathbb{N}_0 \quad \forall(\lambda,\gamma) \in \mathbb{R}^2. \tag{11}$$

The first derivative of $\tau_{\max}(\vartheta)$ can be calculated. Since this function is implicitly defined by zeros of $\varphi(\vartheta, \tau_{\max})$, the first derivative $\mathrm{D}\tau_{\max}/\mathrm{D}\vartheta$ can be obtained by equating to zero the total derivative of $\varphi(\vartheta, \tau_{\max})$:

$$\frac{\mathrm{D}\varphi}{\mathrm{D}\vartheta}(\vartheta,\tau_{\max}) = \left(\frac{\partial\varphi}{\partial\vartheta} + \frac{\partial\varphi}{\partial\tau_{\max}}\frac{\mathrm{D}\tau_{\max}}{\mathrm{D}\vartheta}\right)(\vartheta,\tau_{\max}) = 0,$$

$$\frac{\mathrm{D}\tau_{\max}}{\mathrm{D}\vartheta}(\vartheta,\tau_{\max}) = -\frac{(\partial\varphi/\partial\vartheta)(\vartheta,\tau_{\max})}{(\partial\varphi/\partial\tau_{\max})(\vartheta,\tau_{\max})}.$$

It should be noted that $\mathrm{D}\tau_{\max}/\mathrm{D}\vartheta$ depends on the value of its primitive function $\tau_{\max}(\vartheta)$. Setting $\tau_{\max}^{(k)} = \mathrm{D}^k\tau_{\max}/\mathrm{D}\vartheta^k$ and proceeding with implicit derivation with respect to the ϑ variable, the nth derivative can be calculated:

$$\tau_{\max}^{(1)}(\vartheta,\tau_{\max}) = -\frac{(\partial\varphi/\partial\vartheta)(\vartheta,\tau_{\max})}{(\partial\varphi/\partial\tau_{\max})(\vartheta,\tau_{\max})},$$

$$\tau_{\max}^{(2)}(\vartheta,\tau_{\max}) = \frac{\partial\tau_{\max}^{(1)}}{\partial\vartheta} + \frac{\partial\tau_{\max}^{(1)}}{\partial\tau_{\max}}\tau_{\max}^{(1)} = \left(\frac{\partial}{\partial\vartheta} + \tau_{\max}^{(1)}\frac{\partial}{\partial\tau_{\max}}\right)\tau_{\max}^{(1)},$$

$$\vdots$$

$$\tau_{\max}^{(n)}(\vartheta,\tau_{\max}) = \frac{\partial\tau_{\max}^{(n-1)}}{\partial\vartheta} + \frac{\partial\tau_{\max}^{(n-1)}}{\partial\tau_{\max}}\tau_{\max}^{(1)} = \left(\frac{\partial}{\partial\vartheta} + \tau_{\max}^{(1)}\frac{\partial}{\partial\tau_{\max}}\right)\tau_{\max}^{(n-1)}.$$

The above derivatives have $\tau_{\max}(\vartheta)$ as argument and thus, if the value of this function is known when $\vartheta \to 0$, a Maclaurin series expansion of the unknown function can be obtained in a neighborhood of the chosen point $\vartheta_0 = 0$ or, from another point of view, in a neighborhood of $\mathbf{x}_0 = (\vartheta_0, \tau_{\max}(\vartheta_0)) = (0, n\pi)$:

$$\begin{aligned}\tau_{\max}(\vartheta) &= \underbrace{\tau_{\max}(0)}_{n\pi} + \tau_{\max}^{(1)}|_{\mathbf{x}_0}\vartheta + \frac{\tau_{\max}^{(2)}}{2!}\bigg|_{\mathbf{x}_0}\vartheta^2 + \cdots + \frac{\tau_{\max}^{(n)}}{n!}\bigg|_{\mathbf{x}_0}\vartheta \\ &= n\pi + \sum_{k=1}^{n}\frac{\tau_{\max}^{(k)}}{k!}\bigg|_{\mathbf{x}_0}\vartheta^k.\end{aligned}$$

Remembering that $\vartheta = 1/\tau_d$, we can write:

$$\tau_{\max}(\tau_d) = n\pi + \sum_{k=1}^{n}\frac{\tau_{\max}^{(k)}}{k!}\bigg|_{\mathbf{x}_0}\left(\frac{1}{\tau_d}\right)^k. \tag{12}$$

By truncating the series expansion at the fourth term, a good approximation of the time values corresponding to the maximum displacements can be obtained, for each value of λ and γ. In fact, for each set of constants $(n_0, n_1, n_2, n_3, n_4) \in \mathbb{N}_0^5$, from Eq. (12) we obtain:

$$\tau_{\max}(\tau_d) = n_0\pi + (\lambda+\gamma)\left(\frac{1}{\cos n_1\pi} - 1\right)\left(\frac{1}{\tau_d}\right) - \frac{n_2\pi\gamma(2\lambda+\gamma)}{\cos n_2\pi}\left(\frac{1}{\tau_d}\right)^2$$

$$+\left[\left(2\lambda\gamma^2+3\lambda^2\gamma+\frac{2}{3}\gamma^3-\frac{\lambda^3}{3}\right)\left(\frac{1}{\cos n_3\pi}-1\right)+\frac{(n_3\pi)^2\left(\frac{3}{2}\lambda\gamma^2+\frac{\gamma^3}{2}\right)}{\cos n_3\pi}\right]\left(\frac{1}{\tau_d}\right)^3$$

$$+\frac{n_4\pi\gamma}{6}\left[\left(24\lambda\gamma^2+21\lambda^2\gamma+6\gamma^3\right)\left(2-\frac{1}{\cos n_4\pi}\right)-\frac{21\lambda^2\gamma+(n_4\pi)^2(4\lambda\gamma^2-\gamma^3)}{\cos n_4\pi}\right]\left(\frac{1}{\tau_d}\right)^4. \tag{13}$$

Eq. (13) is shown in Fig. 1, when $\lambda=1$, $\gamma=2.8$ and natural constants have the following values:

$$n_0=0,1,2,3,\quad n_1=0,1,2,3,\quad n_2=0,1,\quad n_3=0,1,\quad n_4=0,1.$$

Since the set of constants (n_0,n_1,n_2,n_3,n_4) corresponding to the absolute maximum displacement cannot be calculated in closed form, in order to build the response spectrum it is necessary to analyze the influence of the natural constants on the dynamic load factor.

2.2. Response spectrum

The response spectrum can be obtained from the solutions of the motion equation for both motion phases, that is the forced vibration phase and the free vibration one. A first empirical assessment for the transient response spectrum can be obtained by building the envelope function generated by enveloping the displacement functions, which are evaluated at $\tau_{\max}$ for several values of $n_0,n_1,\ldots,n_4$. So, when forced vibrations occur, we get:

$$|\mathrm{DLF}_{\max,1}(\tau_d)|=\frac{\tau_d^2}{\gamma^2+\tau_d^2}\left|f_2\frac{\sin\tau_{\max}}{\tau_d}-f_1\cos\tau_{\max}+\left(f_1-\lambda\frac{\tau_{\max}}{\tau_d}\right)\exp\left(-\gamma\frac{\tau_{\max}}{\tau_d}\right)\right|, \tag{14}$$

with $\tau_{\max}$ from Eq. (13). And for free vibrations we have:

$$\begin{cases}|\mathrm{DLF}_{\max,2}(\tau_d)|=\sqrt{\mathrm{A}^2+\mathrm{B}^2},\\ \mathrm{A}=\dfrac{\tau_d^2}{\gamma^2+\tau_d^2}\left\{-f_1+e^{-\gamma}\left[(f_1-\lambda)\cos\tau_d+\dfrac{f_2-\lambda\gamma}{\tau_d}\sin\tau_d\right]\right\},\\ \mathrm{B}=\dfrac{\tau_d^2}{\gamma^2+\tau_d^2}\left\{\dfrac{f_2}{\tau_d}+e^{-\gamma}\left[(f_1-\lambda)\sin\tau_d-\dfrac{f_2-\lambda\gamma}{\tau_d}\cos\tau_d\right]\right\},\end{cases} \tag{15}$$

where $\mathrm{DLF}_{\max,1}$ and $\mathrm{DLF}_{\max,2}$ denote the relative maximum values of dynamic load factor for forced and free vibrations, respectively.

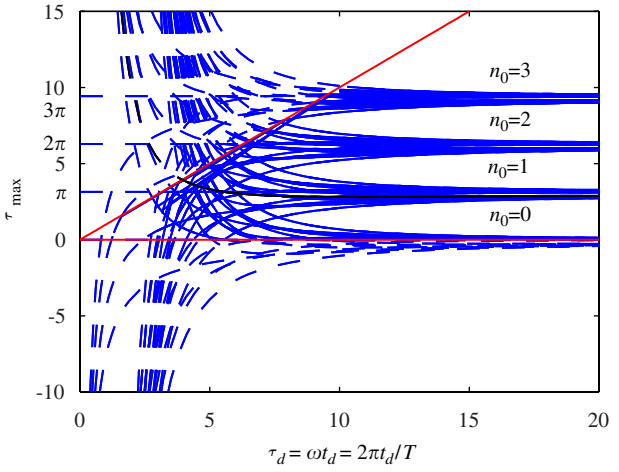

Fig. 1. Exponentially decaying load ($\lambda=1,\gamma=2.8$): times of relative maximum displacement during the forced vibrations phase, varying the load duration. Continuous lines identify the parts of the charts in the time range $(0,\tau_d)$.

For low values of the load duration, the spectrum is determined by free vibrations (Eq. (15)). For high values of τ_d instead, the spectrum is determined by solution (14), with $(n_0,\ldots,n_4)=(1,0,0,0,0)$. Finally, for intermediate values of the load duration, the response can only be obtained varying the values $(n_0,\ldots,n_4)$ and choosing, for each value of τ_d, the maximum displacement. In Figs. 2 and 3 the DLF $-\tau_d$ charts are presented to show the influence of $n_0,\ldots,n_4$ on the response spectrum. The charts are obtained from all the combinations of the following values of natural constants:

for Fig. 2,

$$n_0=0,1,2,3,\quad n_1=0,\quad n_2=0,1,\ldots,6,\quad n_3=0,\quad n_4=0.$$

for Fig. 3,

$$n_0=0,\ldots,10,\quad n_1=0,\ldots,5,\quad n_2=0,\ldots,5,\quad n_3=0,\quad n_4=0.$$

By enveloping a larger number of displacement functions, obtained with wider ranges of natural constants, we get the curves in Figs. 4 and 5. As can be seen in these figures, a descending pulse load originates a concave downward spectrum of displacements, without changes of curvature sign. Numerical results show narrower

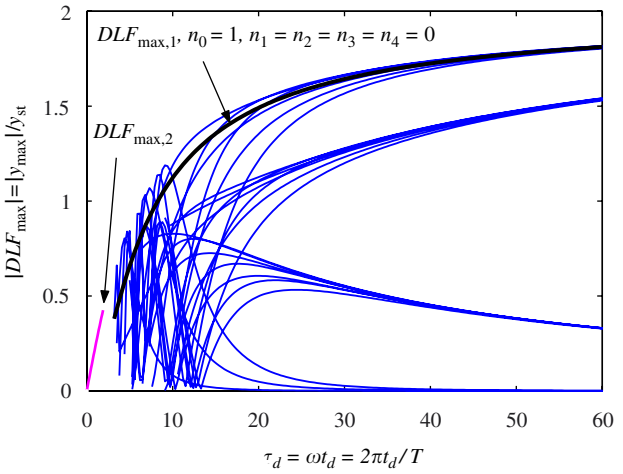

Fig. 2. Exponentially decaying load ($\lambda=1,\gamma=2.8$): displacements determined with 28 different sets of constants $(n_0,\ldots,n_4)$.

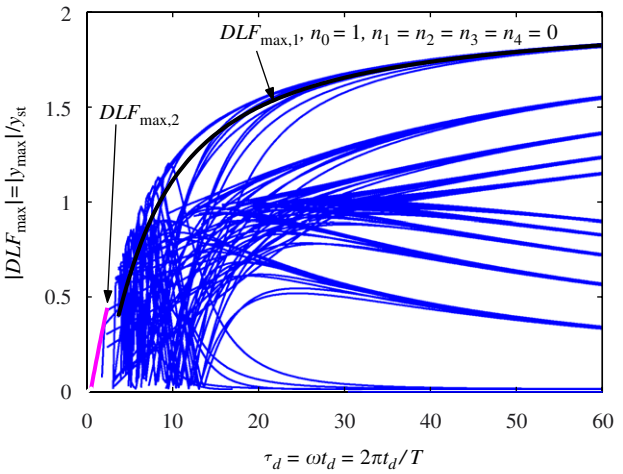

Fig. 3. Exponentially decaying load ($\lambda=1,\gamma=2.8$): displacements determined with 396 different sets of constants $(n_0,\ldots,n_4)$.

zones where the curvature sign changes as the amount of sets of constants used to calculate the spectrum is increased.

In the present paper, the negative sign of the second spectrum derivative is assumed as a hypothesis, and will be called *concavity spectrum hypothesis* or, more shortly, *concavity hypothesis*. Based on this hypothesis, a smoothing algorithm is introduced to adjust the ordinates of those points where the concavity hypothesis is not respected. The algorithm allows a lowering of the computational cost, because it allows to calculate the response spectrum by using a smaller amount of sets of constants $(n_0, \ldots, n_4)$. Results produced by the smoothing algorithm are shown in Figs. 6 and 7. This way, it is possible to eliminate all the changes of curvature in the envelope function.

2.3. Approximate expression of the transient response spectrum

The research of an analytical expression for the response spectrum requires the solution of three problems: the choice of the spectrum domain, the demonstration of the spectrum concavity and the definition of the spectrum transition time.

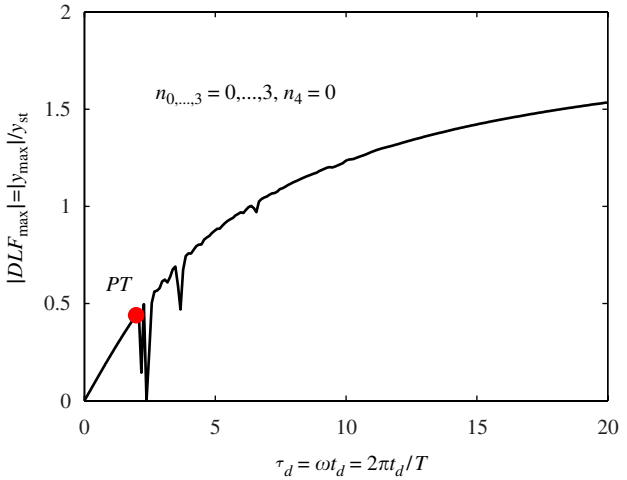

Fig. 4. Envelope function, considering 256 different displacement functions ($\lambda = 1, \gamma = 2.8$).

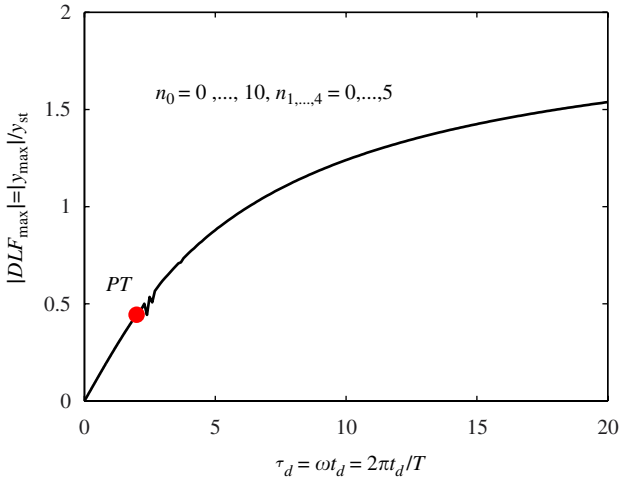

Fig. 5. Envelope function, considering 14 256 different displacement functions ($\lambda = 1, \gamma = 2.8$).

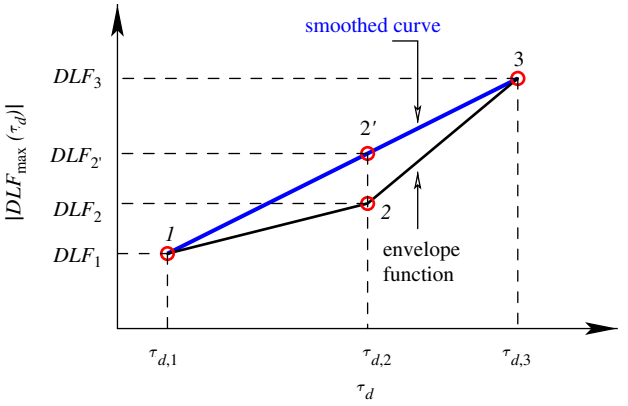

Fig. 6. Smoothing of the response spectrum: the point 2 ordinate is replaced by the point 2' one, calculated by linear interpolation between points 2 and 3.

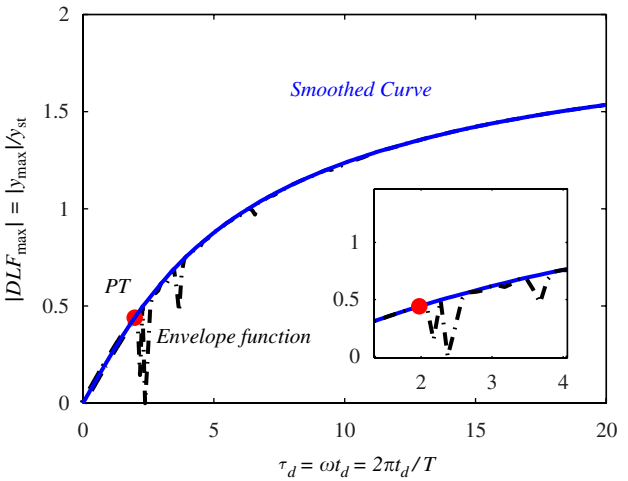

Fig. 7. Envelope function (dash–dot line) and smoothed curve (continuous line).

The choice of the spectrum domain depends on the range in which the natural period of vibration of the loaded structure lies, as well as on the positive phase duration of the blast load. For civil structures, the fundamental period of vibration T can be assumed in the interval [0.1,20] s. For the loading duration of a detonation, Smith and Hetherington [20] suggest $t_d \in [10^{-1}, 10]$ ms, as it is also prescribed in Eurocode 1 [21], which predicts a loading time lower than 10 ms. In case of deflagration, Eurocode 1 suggests a loading time of 100 ms, but in literature various pressure profiles are presented whose positive phase achieves 300 ms [22]. On that account the spectrum domain can be established in the following range:

$$\tau_d = 2\pi \frac{t_d}{T} \in [10^{-5}\pi, 6\pi] \approx [10^{-5}, 20].$$

The concavity hypothesis, which is the basis of the smoothing algorithm introduced in Section 2.2, can be rigorously demonstrated only for rectangular or triangular load shapes, but it is assumed true for each descending pulse load.

The third problem mentioned above concerns the definition of the spectrum transition time $\tau_{d,0}$ which corresponds with the abscissa of the transition point (PT). The first part of the spectrum, near the axis origin

($\tau_d \leqslant \tau_{d,0}$), is generated by free vibrations, and the second one is generated by forced vibrations ($\tau_d > \tau_{d,0}$). For rectangular or triangular pulse shapes, $\tau_{d,0}$ can be analytically established; for each other load shape $\tau_{d,0}$ is assumed coincident with the upper boundary of existence for the first solution of Eq. (8). When $n = 1$ and $\tau_d > \tau_{d,0}$, Eq. (8) predicts $\tau_{\max} < \tau_d$, but when this condition occurs, the motion is forced and Eq. (8) does not work. So, $\tau_{d,0}$ is given by

$$\pi + \arctan(\mathrm{B}/\mathrm{A})|_{\tau_d = \tau_{d,0}} = \tau_{d,0}.$$

When $\tau_d > \tau_{d,0}$, an analytical expression for the response curve can be calculated by the least square method [23], with a polynomial regression on spectrum points. The spectrum shape suggests the use of regression functions as follows:

$$S_r(\tau_d) = a_r \left[2^r - \left(\frac{1}{\tau_d + 0.5} \right)^r \right], \quad r \in \mathbb{N}, \quad a_r \in \mathbb{R}. \tag{16}$$

By adding the first g functions given from Eq. (16), we get an expression $S(\tau_d)$ for the fitted curve, depending on unknown parameters a_r of the analytical model:

$$S(\tau_d) = a_0 - \sum_{r=1}^{g} \frac{a_r}{(\tau_d + 0.5)^r}. \tag{17}$$

In order to join the two curves described from Eqs. (15) and (17), which both represent the system response corresponding to the transition point, the same values of the two functions and their derivatives must be set when $\tau_d = \tau_{d,0}$. After fixing the following positions:

$$X = (\tau_d + 0.5)^{-1}, \quad b_0 = a_0, \quad b_r = -a_r \quad \forall r > 0,$$

$$X_0 = (\tau_{d,0} + 0.5)^{-1}, \quad S_0 = S(\tau_{d,0}), \quad S_0' = S'(\tau_{d,0}) = \tan \alpha_0$$

and when the axis origin is translated into $\mathrm{PT} \equiv (\tau_{d,0}; S(\tau_{d,0}))$:

$$\overline{X} = X - X_0, \quad \overline{S} = S - S_0,$$

we can write:

$$\overline{S} = \sum_{r=0}^{g} b_r \overline{X}^r, \tag{18}$$

where b_r are the new unknown parameters that have to be estimated. Then, by fixing the ordinate of the spectrum and the slope of his tangent line at $\tau_d = \tau_{d,0}$, we get:

$$\bar{S}(0) = \sum_{r=0}^{g} b_r \bar{X}^r \bigg|_{\bar{X}=0} = b_0 = 0 \tag{19}$$

and also

$$\left. \frac{\mathrm{d}\bar{S}}{\mathrm{d}\tau_d} \right|_{\tau_d = \tau_{d,0}} = \tan \alpha_0 \quad \Rightarrow \quad b_1 = -(\tau_{d,0} + 0.5)^2 \tan \alpha_0. \tag{20}$$

The overdetermined system (18) becomes:

$$S - S_0 + (\tau_{d,0} + 0.5)^2 \tan \alpha_0 = \sum_{r=2}^{g} b_r (X - X_0)^r. \tag{21}$$

When system (21) is solved, the expression of the transient response spectrum is given by

$$S(\tau_d) = S(\tau_{d,0}) - (\tau_{d,0}+0.5)^2 \tan\alpha_0 \left(\frac{1}{\tau_d+0.5} - \frac{1}{\tau_{d,0}+0.5}\right) + \sum_{r=2}^{g} b_r \left(\frac{1}{\tau_d+0.5} - \frac{1}{\tau_{d,0}+0.5}\right)^r \quad \forall \tau_d > \tau_{d,0}. \tag{22}$$

If τ_d and the constants $n_{0,1,\ldots,4}$ have the following values:

$$\tau_d = \tau_{d,0}, \tau_{d,0}+0.1, \tau_{d,0}+0.2, \ldots, 20,$$
$$n_{0,1,2,3} = 0, 1, 2, 3,$$
$$n_4 = 0$$

we get the fitted curve shown in Figs. 8 and 9. The regression parameters are presented in Table 1.

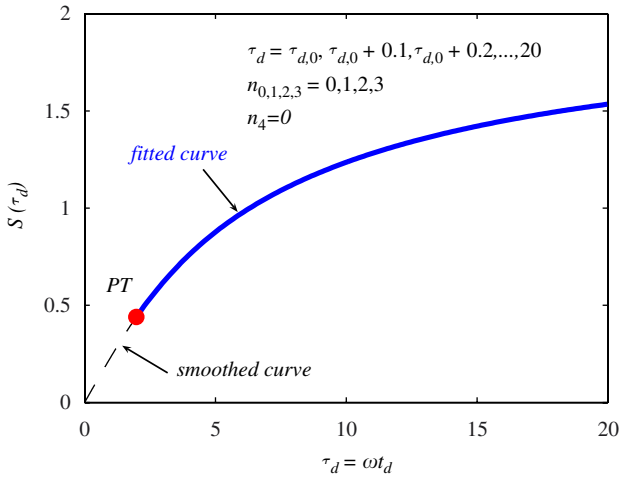

Fig. 8. Regression function of the response spectrum ($\lambda = 1,\ \gamma = 2.8$).

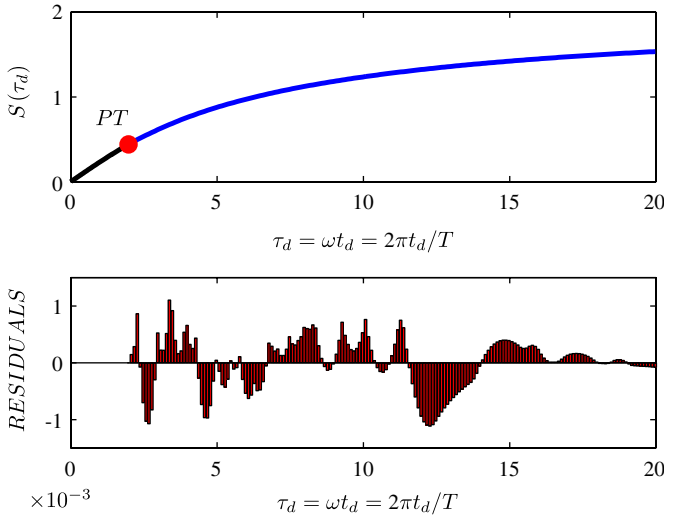

Fig. 9. Residuals distribution ($\lambda = 1,\ \gamma = 2.8$).

Table 1
Response spectrum ($\lambda = 1,\ \gamma = 2.8$): coefficients of the regression polynomial of sixth degree

$\tau_d = [\tau_{d,0}, \tau_{d,0} + 0.1, \tau_{d,0} + 0.2, \ldots, 20],\ n_{0,1,2,3} = 0, 1, 2, 3,\ n_4 = 0$	
r	b_r
0	0.0000
1	−1.1933e+000
2	1.4487e+000
3	−1.0797e+001
4	−5.8500e+000
5	4.6883e+001
6	1.8058e+002

2.4. Influence of computation parameters on response spectrum

The coefficients b_r in Eq. (22), obtained by solving system (21), are strongly influenced by the following computation parameters:

(1) the values assigned to $(n_0, n_1, n_2, n_3, n_4)$ which give a numerical assessment of Eqs. (13) and (14), and thus decide the ordinates of the envelope function;
(2) the choice of points in the spectrum domain, which have a strong influence on the polynomial regression;
(3) the choice of the regression functions to model the response $S(\tau_d)$ and apply the least squares method.

Fig. 10 shows a possible convergence of the coefficients b_r as the amount of computed sets of constants $n_{0,\ldots,4}$ is increased, as well as the variation of the spectrum chart. But these results are not definitive and can only show a trend of the response depending on the set $(n_0, \ldots, n_4)$. Therefore, to improve the knowledge about the existing relation between $n_{0,\ldots,4}$ and the response curve, it could be necessary to use statistical techniques like design of experiment (robust design) and response surfaces.

In order to choose the points within the transient spectrum domain $[\tau_{d,0}, 20]$, an evident convergence of b_r can be noted as the mesh approaches zero, if a uniform domain partition is considered, as shown in Fig. 11.

Finally, a regression function for the response curve must satisfy some fundamental requirements.

Firstly, the quality of the fit is acceptable when the standardized residuals are normal and (approximately) independently distributed with a zero mean and with $[-1.96, 1.96]$ as confidence interval, with about 95% of confidence level (Fig. 9).

Secondly, under ideal circumstances, a plot of the residuals must show no geometric regularity, as it verified. It is worth noting that expression in Eq. (22) has these features.

In order to define the degree of the polynomial $S(\tau_d)$, it has to be noted that, as the degree is increased, we get a badly conditioned system solving the least squares problem. Moreover, with a sixth degree polynomial, the residuals values obtained are very low and decreasing while the amount of sets $n_{0,\ldots,4}$ used to make the envelope-function increases. In fact, when the argument $\overline{X}$ of the rth power in $S(\tau_d)$ is lesser than the unity, the influence of b_r decreases as r goes up. This condition is always verified when $\tau_{d,0} > 0.5$ (Fig. 12), as it happens when $\lambda \in [0, 1]$ and $\gamma \in [0, 10]$.

3. Structural damage and p–i diagram

Let us suppose y_c to be a critical displacement corresponding to structural failure. If the resistance function of the spring is linear until failure (elastic-fragile behavior), the damage level can be defined by the following ratio:

$$d = \frac{|y_{\max}|}{y_c}, \tag{23}$$

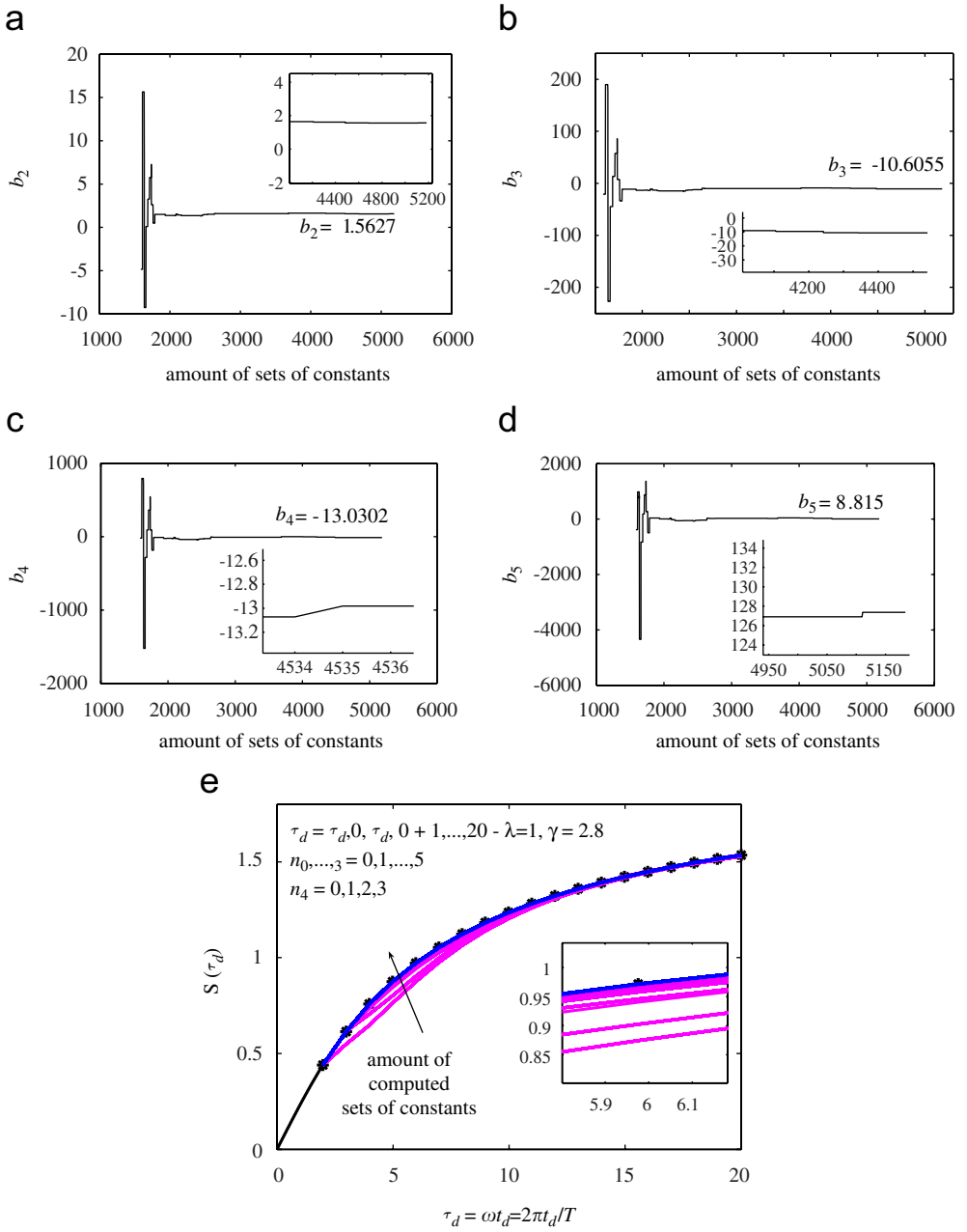

Fig. 10. Influence of the amount of the computed sets of constants on the regression function $S(\tau_d)$: (a) variation of b_2, (b) variation of b_3, (c) variation of b_4, (d) variation of b_5, (e) variation of spectrum chart.

where $|y_{\max}|$ is the absolute maximum displacement. It should be noted that a "real damage" of the system occurs only when $d = 1$. When $d < 1$ the elastic deformation is recovered by the spring, and so d^{-1} can be regarded as a safety factor against the failure. In order to represent the damage level it is convenient to define the following dimensionless pressure and impulse:

$$p = \frac{F_{\max}}{F_0}, \tag{24a}$$

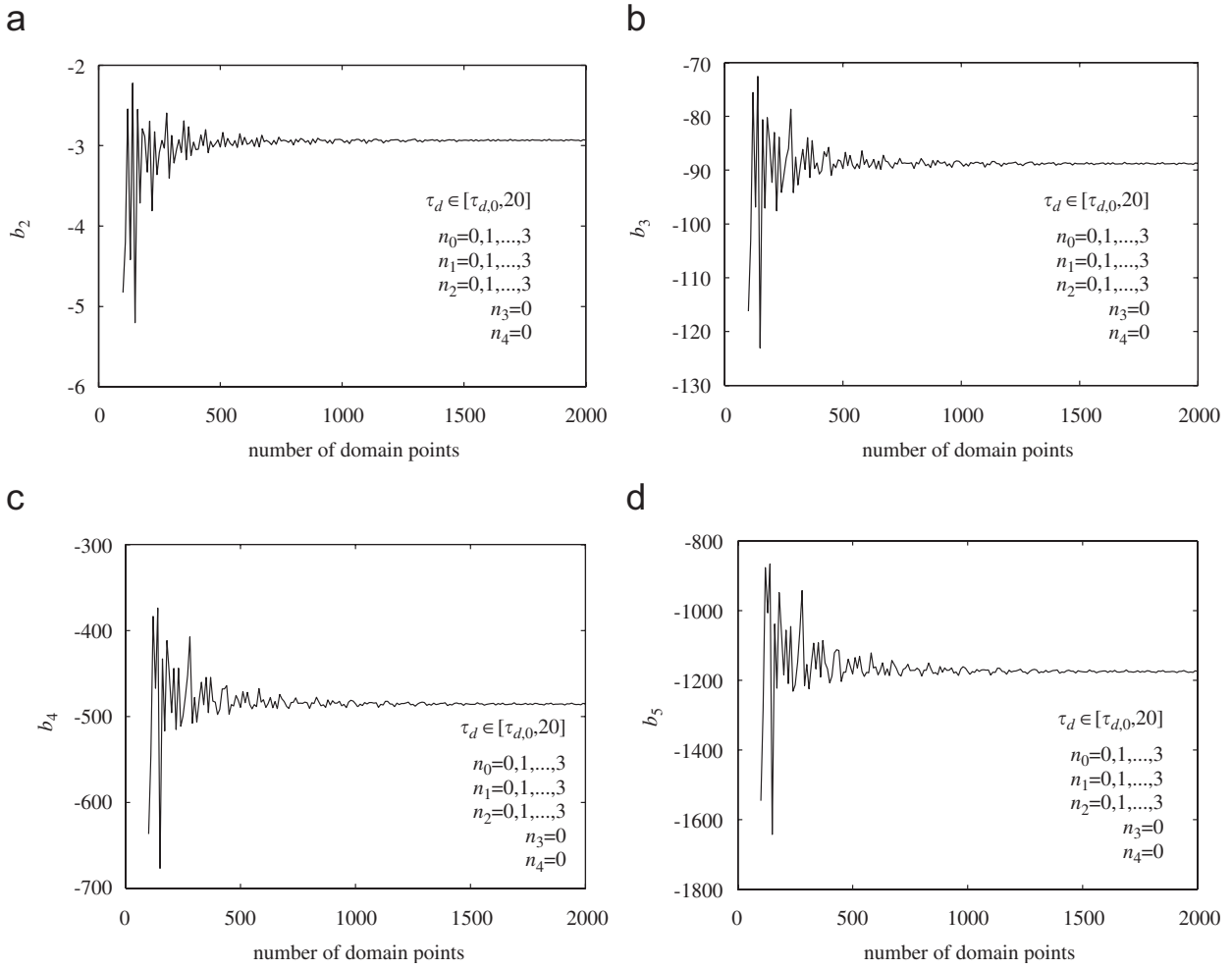

Fig. 11. Convergence of b_k varying the partition of the spectrum domain when $\lambda = 1$ and $\gamma = 2.8$: (a) convergence of b_2, (b) convergence of b_3, (c) convergence of b_4, (d) convergence of b_5.

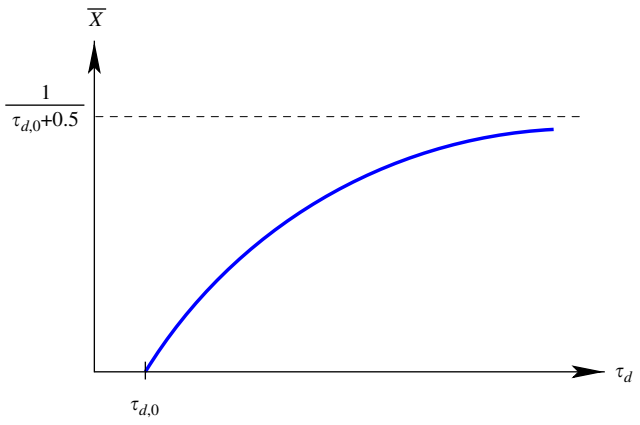

Fig. 12. Variation of the argument of rth power in spectrum expression varying load duration.

$$i = \frac{I}{I_0}, \tag{24b}$$

where $0.5F_0 = 0.5y_c k$ is the magnitude of the step load that produces the specified critical displacement y_c and $I_0 = y_c\sqrt{mk}$ is the ideal impulse that produces the same displacement. Once the analytical expression of $S(\tau_d)$ is known from Eqs. (15) and (22), and remembering the definition of $\mathrm{DLF}_{\max}$ and the impulse expression from Eq. (2), the structural damage level can be shown as a function with four variables:

$$d = G(p, i, \lambda, \gamma) = p \cdot S(\tau_d), \quad \tau_d = \frac{i}{p}\psi(\lambda, \gamma)^{-1}. \tag{25}$$

Fig. 13 shows the surface given from Eq. (25), generated by an exponentially decaying load ($\lambda = 1,\ \gamma = 8$). The level curves of this surface, where the G function takes on given constant values, are the well-known isodamage curves, which represent the set of the points in the pressure–impulse space that correspond to all the different loads, of fixed pulse shape, which produce a damage level equal to d. The isodamage curves, given implicitly from Eq. $G(p, i, \lambda, \gamma) = \text{const.}$, can be represented in explicit form as parametric curves with respect

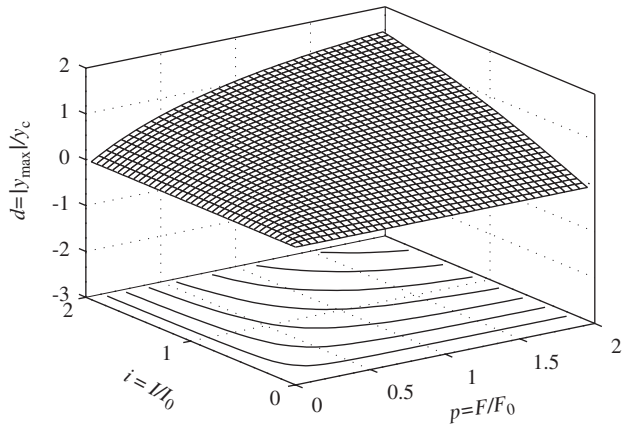

Fig. 13. Damage function ($\lambda = 1,\ \gamma = 2.8$); under surface some level curves given by $d = \text{constant}$ are reported.

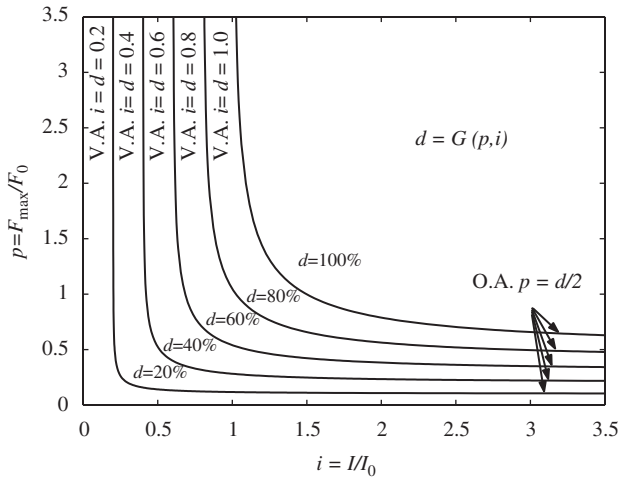

Fig. 14. Isodamage curves corresponding to 5 different damage levels ($\lambda = 1,\ \gamma = 2.8$).

to the parameter τ_d (Fig. 14):

$$p = \frac{d}{S(\tau_d)}, \quad i = p \cdot \tau_d \cdot \psi(\lambda, \gamma). \tag{26}$$

3.1. Response limits

Generally a p–i diagram is not a monotonically decreasing function. This is not the case, for example, when the loading pressure profile has a finite rise time, or when the negative loading phase cannot be neglected, as shown by Baker et al. [1]. When the loading pressure profile is monotonically decreasing, e.g. when $\lambda \in [0, 1]$ and $\gamma \in [0, 10]$, the isodamage curves are monotonically decreasing and they have vertical and horizontal asymptotes. These asymptotes can be established via an energy criterion. The energy balance for the spring–mass system at a generic time is given by

$$W_e = \Phi + \mathrm{T}, \tag{27a}$$

$$\int_0^t F(t')\dot{y}(t')\,\mathrm{d}t' = \frac{1}{2}ky^2(t) + \frac{1}{2}m\dot{y}^2(t), \tag{27b}$$

in which W_e represents the work done by external load, T is the kinetic energy of the system and Φ is the elastic strain energy of the spring.

For an impulsive load, the equation of the impulsive asymptote is deduced from Eq. (27):

$$|\mathrm{T}(0)| = |\Phi_{\max}|,$$

$$\frac{I^2}{2m} = \frac{1}{2}ky_{\max}^2(t),$$

$$i = \frac{I}{I_0} = d. \tag{28}$$

On the other hand, for a quasi-static load (step rise, constant magnitude, step decaying), the equation of the quasi-static asymptote can be obtained as follows:

$$\int_0^{t_{\max}} F\dot{y}(t)\,\mathrm{d}t = \frac{1}{2}ky^2(t_{\max}) + \frac{1}{2}m\dot{y}^2(t_{\max}),$$

$$Fy_{\max} = \frac{1}{2}ky_{\max}^2, \quad y_{\max} = y(t_{\max}),$$

$$p = \frac{F}{F_0} = \frac{d}{2}. \tag{29}$$

Generally, all charts relative to a given pulse shape can be conventionally divided into three regions, depending on the ratio of load duration to fundamental period of the structures:

$$\frac{t_d}{T} = \frac{\tau_d}{2\pi}. \tag{30}$$

For low values of τ_d, a p–i curve collapses into its vertical asymptote, and the response is similar to that one of a system excited by an impulsive load. This regime is called impulsive (I). For high values of τ_d the diagram collapse into its horizontal asymptote, like a system excited by a quasi-static load, corresponding to a quasi-static regime (III). Finally, for intermediate values of this ratio, the system response can be calculated only with a rigorous dynamic analysis; it corresponds to the dynamic regime (II). Points A and B on the p–i curve, corresponding to a transition from a kind of regime to another, have been established by Li and Meng with a 5% relative accuracy about the values of the horizontal and vertical asymptotes, as shown in Fig. 15.

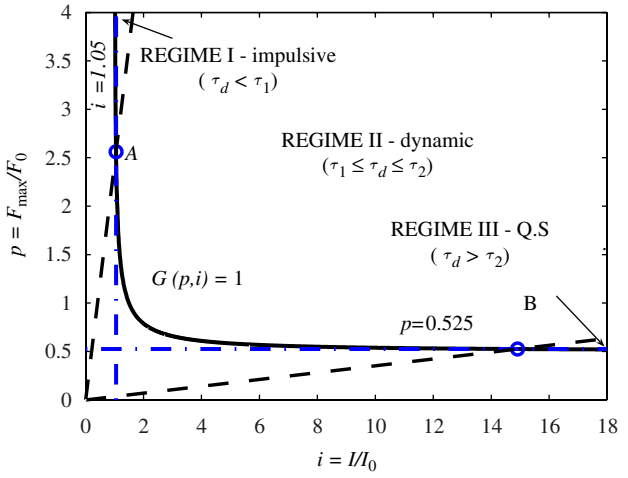

Fig. 15. Response regimes ($\lambda = 1$, $\gamma = 2.8$): impulsive, dynamic (A–B portion), quasi-static.

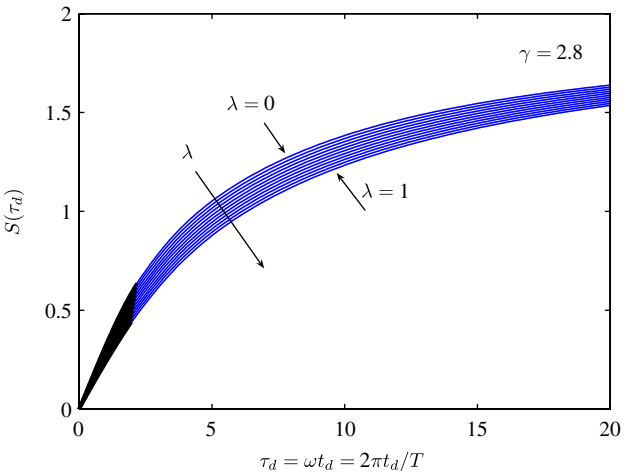

Fig. 16. Influence of load shape on response spectrum; $\gamma = 2.8$, $\lambda = 0, 0.1, 0.2, \ldots, 1$.

3.2. Pulse shape effects on the system response

The influence of the pulse shape on the structural response is shown in Figs. 16–19. When λ and γ increase, the response spectrum moves down progressively and slowly approaches the horizontal asymptote (DLF = 2). The isodamage curves move away from the origin and their length in dynamic regime increases.

3.3. Regression model for isodamage curves

When the response spectrum is known, the consequent expression derived for p–i diagrams is rather complex. In fact, from Eqs. (15), (22) and (26), we get:

$$\begin{cases} p = \dfrac{d}{\sqrt{A^2 + B^2}} \\ i = p\tau_d\psi(\lambda,\gamma) \end{cases} \quad \text{for } \tau_d \leqslant \tau_{d,0}, \tag{31}$$

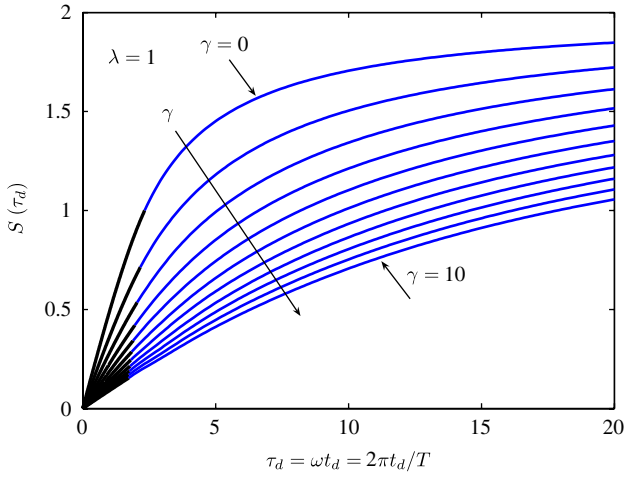

Fig. 17. Influence of load shape on response spectrum; $\lambda = 1$, $\gamma = 0, 1, 2, \ldots, 10$.

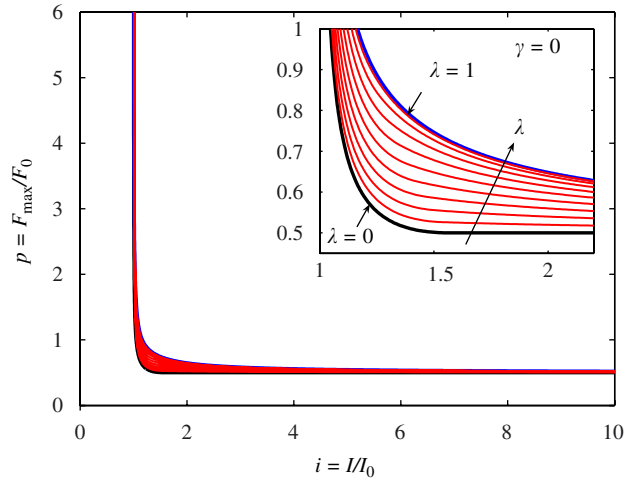

Fig. 18. Influence of load shape on p–i diagrams; $\lambda = 0, 0.1, 0.2, \ldots, 1$, $\gamma = 0$, $d = 1$.

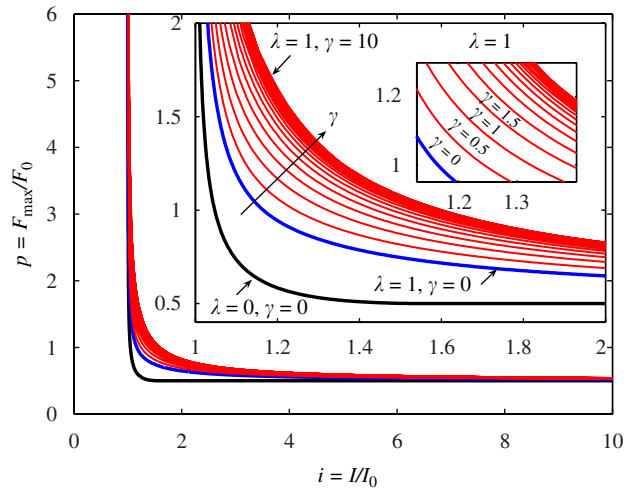

Fig. 19. Influence of load shape on p–i diagrams; $\gamma = 0, 0.5, 1.0, \ldots, 10$, $\lambda = 1$, $d = 1$.

$$\begin{cases} p = \dfrac{d}{S_0 + \sum_{r=1}^{g} b_r \left(\dfrac{1}{\tau_d + 0.5} - \dfrac{1}{\tau_{d,0} + 0.5} \right)^r} & \text{for } \tau_d > \tau_{d,0}. \\ i = p\tau_d \psi(\lambda, \gamma) \end{cases} \tag{32}$$

In order to find a simplified representation, the curve shape suggests the use of hyperbolic regression functions, like those proposed by Li and Meng:

$$p = \frac{1}{2} + \frac{m_1}{(i-1)^{m_2}}, \tag{33}$$

which can be linearized as follows:

$$Y = \bar{m}_1 + m_2 X, \quad \begin{cases} X = -\ln(i-1), \\ Y = \ln(p - 0.5), \\ \bar{m}_1 = \ln(m_1), \end{cases} \tag{34}$$

where m_1 and m_2 are unknown parameters that are to be estimated. In order to avoid an excessive discrepancy between regression functions and input data, caused by the asymptotic behavior, it is convenient to assign at the jth input point a weight w_j depending on the chart slope at the same point:

$$w_j = \left(\max \left\{ \left| \frac{\mathrm{d}p}{\mathrm{d}i} \right|_{(i_j, p_j)}, \left| \frac{\mathrm{d}i}{\mathrm{d}p} \right|_{(i_j, p_j)} \right\} \right)^v \tag{35}$$

in which the power v is chosen by minimizing the sum of squared residuals (Q^2), considering the deviations η_j on both X and Y directions:

$$Q = \sqrt{\sum_j \eta_j^2}, \quad \eta_j = \min \left\{ |Y_j - (\bar{m}_1 + m_2 X_j)|, \left| X_j - \frac{Y_j - \bar{m}_1}{m_2} \right| \right\}. \tag{36}$$

When the pressure profile is exponentially decaying ($\lambda = 1, \gamma = 2.8$), with $v = 0.90$ we obtain a minimum local point of Q, as shown in Tables 2 and 3 (Fig. 20). By following the same procedure for other load shapes, we get the values of $m_{1,2}$ in Table 4. Certainly, even these results are strongly influenced by the choices of the spectrum domain and sets $n_0, n_1, \ldots, n_4$. Similar problems occur when a relationship has to be estimated between $m_{1,2}$ and the load shape, represented by its centroid. From Eq. (1), and introducing the following change of variables:

$$\xi = \frac{t}{t_d},$$

Table 2
Simplified p–i curves: local minimum of sum of squared deviations; $\lambda = 1$, $\gamma = 2.8$, $d = 1$

v	Q
−0.95	0.3016
−0.94	0.3015
−0.93	0.3015
−0.92	0.3014
−0.91	0.3014
−0.90	**0.3014**
−0.89	0.3014
−0.88	0.3014
−0.87	0.3015
−0.86	0.3015
−0.85	0.3016

Table 3
Regression parameters of p–i diagram; $\lambda = 1$, $\gamma = 2.8$, $d = 1$

$v = -0.90$			Li and Meng (2002)		
m_1	m_2	Q	m_1	m_2	Q
0.305	0.693	0.301	0.300	0.700	0.301

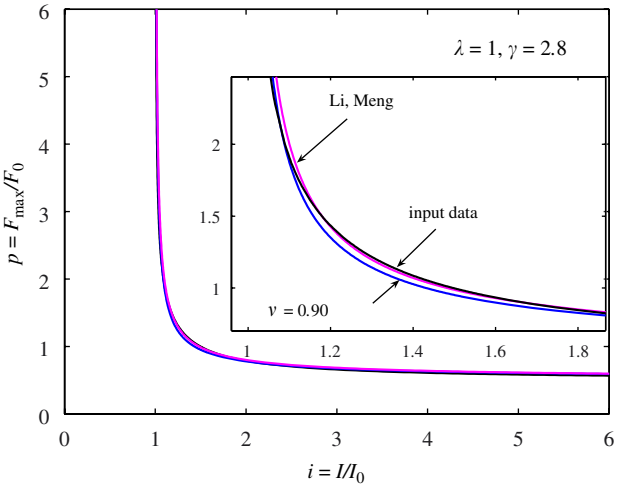

Fig. 20. Simplified p–i diagram; $\lambda = 1$, $\gamma = 2.8$, $d = 1$.

the loading function, normalized with respect to his maximum value, becomes:

$$f(\xi) = \begin{cases} (1 - \lambda\xi)\exp(-\gamma\xi) & \text{for } 0 \leqslant \xi \leqslant 1, \\ 0 & \text{for } \xi > 1. \end{cases} \tag{37}$$

The centroid position is given by

$$\xi_0 = \frac{\int_0^1 \xi f(\xi)\,\mathrm{d}\xi}{\int_0^1 f(\xi)\,\mathrm{d}\xi}, \quad \zeta_0 = \frac{\int_0^1 f^2(\xi)\,\mathrm{d}\xi}{2\int_0^1 f(\xi)\,\mathrm{d}\xi}, \tag{38a}$$

$$D = \sqrt{\xi_0^2 + \zeta_0^2}. \tag{38b}$$

By using the quadratic approximation proposed by Li and Meng [2]

$$\begin{aligned} m_1(D) &= \beta_{0,1} + \beta_{1,1}D + \beta_{2,1}D^2, \\ m_2(D) &= \beta_{0,2} + \beta_{1,2}D + \beta_{2,2}D^2 \end{aligned} \tag{39}$$

and from results in Table 4, we get the $\beta_{i,j}$ values which, as suggested by Florek and Benaroya [24], are very different from the values determined by only three load shapes:

$$\begin{aligned} \beta_{0,1} &= 0.654, \quad \beta_{1,1} = -0.936, \quad \beta_{2,1} = 0.002, \\ \beta_{0,2} &= 2.553, \quad \beta_{1,2} = -8.237, \quad \beta_{2,2} = 8.721, \end{aligned}$$

Charts of $m_1(D)$ and $m_2(D)$ are shown in Figs. 21 and 22. A clear relationship can be observed only when one of the shape parameters, λ or γ, is fixed. Therefore, for further research of a simplified expression for p–i diagrams, it could be necessary to establish a relation between $m_{1,2}$ and the load shape in which λ and γ are

Table 4
Parameters of p–i regression functions and response limits ($\varepsilon = 5\%$) corresponding to different pulse shapes

λ	γ	m_1	m_2	τ_1	τ_2	p_A	i_B
0.00	0.000	0.035	0.859	1.077	2.5	0.98	1.32
1.00	0.000	0.141	0.722	1.322	32.3	1.59	8.49
0.05	0.001	0.011	1.344	1.077	2.7	1.00	1.39
0.05	1.001	0.169	0.580	1.107	33.0	1.53	10.72
0.05	2.001	0.275	0.620	1.193	64.4	2.07	14.36
0.05	3.001	0.323	0.695	1.330	95.8	2.53	15.70
0.10	0.001	0.017	1.163	1.077	3.3	1.03	1.63
0.10	1.001	0.176	0.580	1.111	34.6	1.56	11.00
0.10	2.001	0.279	0.623	1.199	66.0	2.10	14.46
0.10	3.001	0.324	0.699	1.339	97.4	2.55	15.74
0.15	0.001	0.026	1.019	1.078	4.9	1.05	2.37
0.15	1.001	0.183	0.582	1.115	36.2	1.59	11.26
0.15	2.001	0.282	0.626	1.206	67.6	2.12	14.55
0.15	3.001	0.325	0.703	1.349	99.0	2.57	15.76
0.20	0.001	0.035	0.912	1.079	6.5	1.08	3.07
0.20	1.001	0.189	0.585	1.119	37.8	1.62	11.49
0.20	2.001	0.285	0.630	1.213	69.2	2.15	14.62
0.20	3.001	0.325	0.706	1.359	100.6	2.59	15.78
0.25	0.001	0.045	0.836	1.081	8.1	1.11	3.73
0.25	1.001	0.195	0.588	1.124	39.4	1.65	11.70
0.25	2.001	0.288	0.635	1.221	70.8	2.18	14.68
0.25	3.001	0.326	0.710	1.370	102.2	2.60	15.80
0.30	0.001	0.054	0.783	1.083	9.7	1.14	4.34
0.30	1.001	0.201	0.592	1.130	41.0	1.68	11.89
0.30	2.001	0.291	0.639	1.230	72.4	2.20	14.73
0.30	3.001	0.326	0.713	1.382	103.8	2.62	15.80
0.35	0.001	0.064	0.744	1.085	11.3	1.17	4.91
0.35	1.001	0.207	0.595	1.136	42.6	1.71	12.06
0.35	2.001	0.293	0.644	1.240	74.0	2.23	14.77
0.35	3.001	0.326	0.716	1.395	105.4	2.64	15.80
0.40	0.001	0.073	0.716	1.089	13.0	1.21	5.46
0.40	1.001	0.212	0.599	1.143	44.2	1.75	12.21
0.40	2.001	0.295	0.648	1.251	75.6	2.25	14.80
0.40	3.001	0.326	0.719	1.410	107.0	2.65	15.79
0.45	0.001	0.083	0.694	1.093	14.6	1.24	5.94
0.45	1.001	0.218	0.603	1.152	45.8	1.78	12.33
0.45	2.001	0.296	0.653	1.264	77.0	2.27	14.77
0.45	3.001	0.325	0.721	1.425	108.4	2.66	15.74
0.50	0.001	0.092	0.677	1.098	16.2	1.28	6.38
0.50	1.001	0.222	0.607	1.161	47.4	1.81	12.44
0.50	2.001	0.297	0.658	1.277	78.6	2.30	14.77
0.50	3.001	0.325	0.724	1.442	110.0	2.68	15.72
0.55	0.001	0.101	0.663	1.104	17.8	1.31	6.77
0.55	1.001	0.227	0.612	1.172	49.0	1.84	12.52
0.55	2.001	0.298	0.663	1.292	80.2	2.32	14.76
0.55	3.001	0.324	0.726	1.461	111.6	2.68	15.69
0.60	0.001	0.110	0.653	1.112	19.4	1.35	7.13
0.60	1.001	0.231	0.618	1.185	50.6	1.87	12.58
0.60	2.001	0.298	0.668	1.310	81.8	2.34	14.74
0.60	3.001	0.323	0.727	1.481	113.2	2.69	15.65
0.65	0.001	0.119	0.648	1.122	21.0	1.39	7.44
0.65	1.001	0.234	0.624	1.201	52.2	1.90	12.61
0.65	2.001	0.298	0.673	1.329	83.4	2.35	14.70
0.65	3.001	0.321	0.729	1.504	114.8	2.70	15.60
0.70	0.001	0.127	0.648	1.134	22.6	1.43	7.71
0.70	1.001	0.236	0.630	1.218	53.8	1.93	12.62
0.70	2.001	0.297	0.678	1.351	85.0	2.37	14.65

Table 4 (*continued*)

λ	γ	m_1	m_2	τ_1	τ_2	p_A	i_B
0.70	3.001	0.320	0.730	1.529	116.4	2.70	15.55
0.75	0.001	0.134	0.652	1.149	24.2	1.46	7.94
0.75	1.001	0.238	0.636	1.239	55.4	1.95	12.62
0.75	2.001	0.296	0.684	1.376	86.6	2.38	14.59
0.75	3.001	0.318	0.730	1.558	118.0	2.70	15.48
0.80	0.001	0.140	0.656	1.168	25.8	1.50	8.13
0.80	1.001	0.239	0.642	1.264	57.0	1.98	12.59
0.80	2.001	0.294	0.687	1.405	88.2	2.38	14.51
0.80	3.001	0.316	0.730	1.589	119.6	2.69	15.41
0.85	0.001	0.145	0.660	1.193	27.6	1.53	8.33
0.85	1.001	0.239	0.647	1.293	58.6	1.99	12.53
0.85	2.001	0.292	0.690	1.439	89.8	2.38	14.43
0.85	3.001	0.314	0.730	1.625	121.2	2.68	15.34
0.90	0.001	0.149	0.664	1.224	29.2	1.56	8.43
0.90	1.001	0.238	0.650	1.330	60.2	2.00	12.46
0.90	2.001	0.289	0.691	1.479	91.4	2.38	14.33
0.90	3.001	0.312	0.729	1.666	122.8	2.66	15.25
0.95	0.001	0.151	0.667	1.266	30.8	1.58	8.49
0.95	1.001	0.237	0.651	1.375	61.8	2.00	12.36
0.95	2.001	0.287	0.690	1.526	93.0	2.36	14.22
0.95	3.001	0.310	0.726	1.713	124.4	2.64	15.16
1.00	0.001	0.152	0.668	1.322	32.4	1.59	8.50
1.00	1.001	0.234	0.650	1.433	63.4	1.99	12.24
1.00	2.001	0.284	0.687	1.582	94.6	2.34	14.09
1.00	3.001	0.307	0.724	1.767	126.0	2.61	15.06

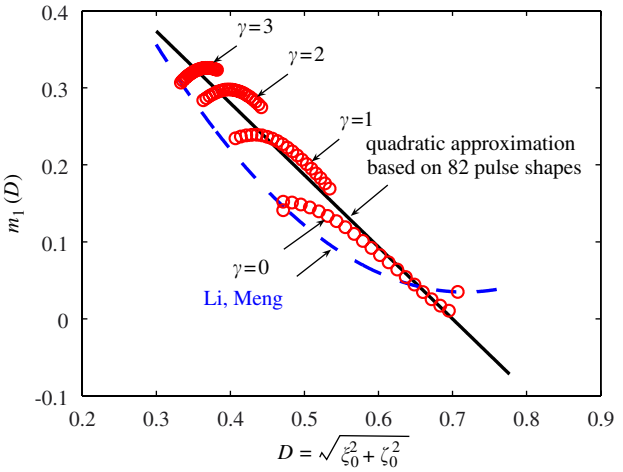

Fig. 21. Quadratic approximation for m_1; ($\lambda = 1$, $\gamma = 2.8$, $d = 1$).

partially uncoupled:

$$m_i = f_i(\lambda) + g_i(\gamma) + h_i(\lambda, \gamma), \quad i = 1, 2.$$

Similar problems occur while investigating the influence of the load shape on the response limits. Even in this case, the quadratic approximation proposed by Li and Meng (Eq. (40)) produces different results if it is applied to the wide range of load shapes in Table 4, and all observations made for $m_{1,2}(D)$ functions about the

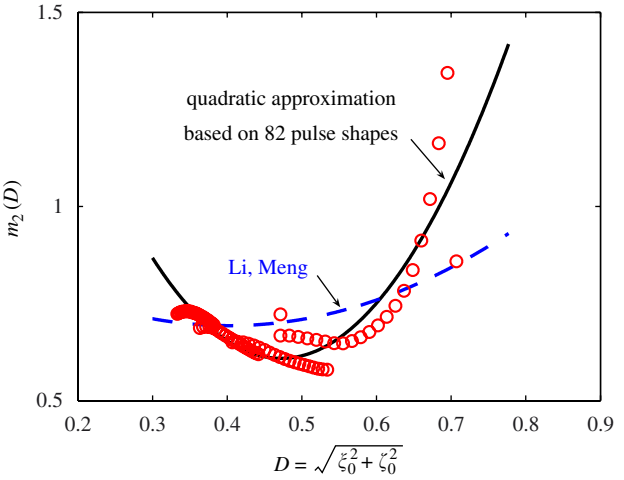

Fig. 22. Quadratic approximation for m_2; ($\lambda = 1$, $\gamma = 2.8$, $d = 1$).

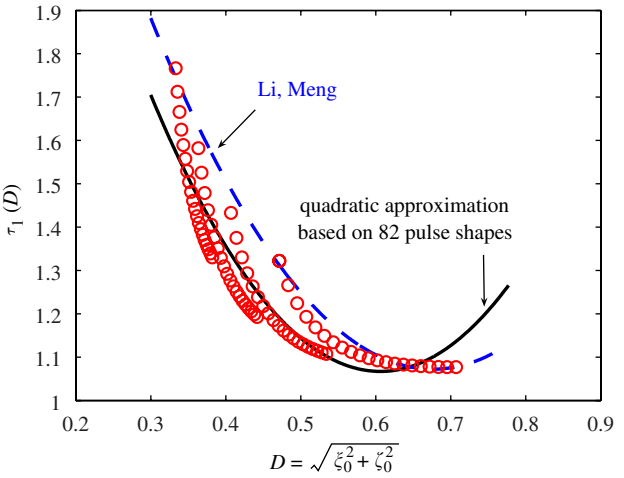

Fig. 23. Quadratic approximation for τ_1; ($\lambda = 1$, $\gamma = 2.8$, $d = 1$).

accuracy of the employed method are still valid:

$$\begin{aligned}
\tau_1(D) &= \beta_{0,\tau_1} + \beta_{1,\tau_1} D + \beta_{2,\tau_1} D^2,\\
\tau_2(D) &= \beta_{0,\tau_2} + \beta_{1,\tau_2} D + \beta_{2,\tau_2} D^2,\\
p_A(D) &= \beta_{0,p_A} + \beta_{1,p_A} D + \beta_{2,p_A} D^2,\\
i_B(D) &= \beta_{0,i_B} + \beta_{1,i_B} D + \beta_{2,i_B} D^2.
\end{aligned} \tag{40}$$

The regression curves of these functions are represented in Figs. 23–26, which are defined using the following β–values:

$$\begin{aligned}
&\beta_{0,\tau_1} = 3.566, \quad \beta_{1,\tau_1} = -8.247, \quad \beta_{2,\tau_1} = 6.803,\\
&\beta_{0,\tau_2} = 475.734, \quad \beta_{1,\tau_2} = -1407.286, \quad \beta_{2,\tau_2} = 1055.256,\\
&\beta_{0,p_A} = 6.745, \quad \beta_{1,p_A} = -15.133, \quad \beta_{2,p_A} = 9.901,\\
&\beta_{0,i_B} = 19.156, \quad \beta_{1,i_B} = 6.332, \quad \beta_{2,i_B} = -46.496.
\end{aligned}$$

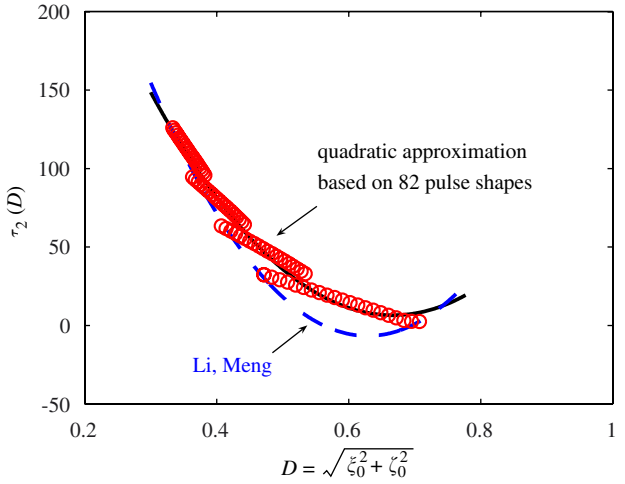

Fig. 24. Quadratic approximation for τ_2; ($\lambda = 1$, $\gamma = 2.8$, $d = 1$).

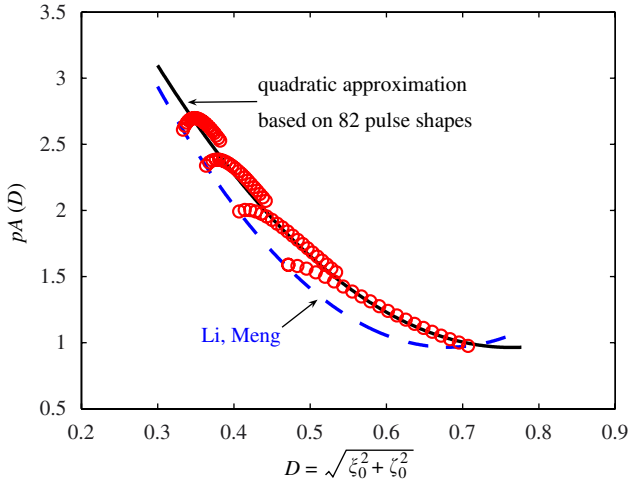

Fig. 25. Quadratic approximation for p_A; ($\lambda = 1$, $\gamma = 2.8$, $d = 1$).

3.4. *Effective pressure–impulse diagram*

In the following the effective impulse is defined in a different way with respect to that shown in Ref. [2]:

$$i_e = 1 + \frac{(i-1)^{m_2}}{m_1} \tag{41}$$

and the same definition is used for the effective pressure

$$p_e = p. \tag{42}$$

Substituting Eqs. (41) and (42) into Eq. (33), we obtain a p_e–i_e curve for a 100% damage level which is shifted towards the p direction by 0.5 with respect to that proposed by Li and Meng:

$$p_e = \frac{1}{i_e - 1} + \frac{1}{2}. \tag{43}$$

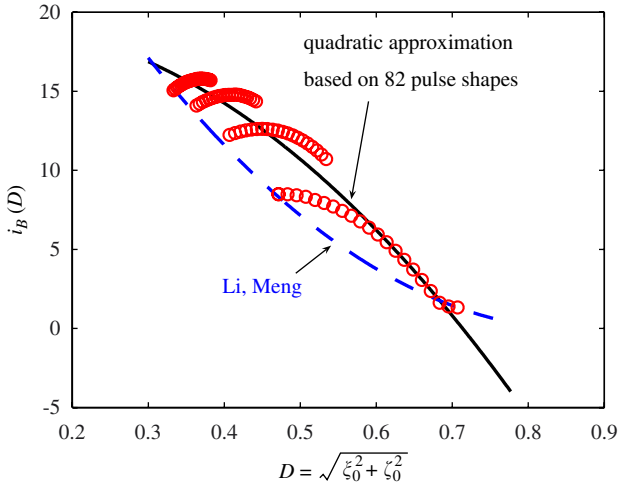

Fig. 26. Quadratic approximation for i_B; ($\lambda = 1$, $\gamma = 2.8$, $d = 1$).

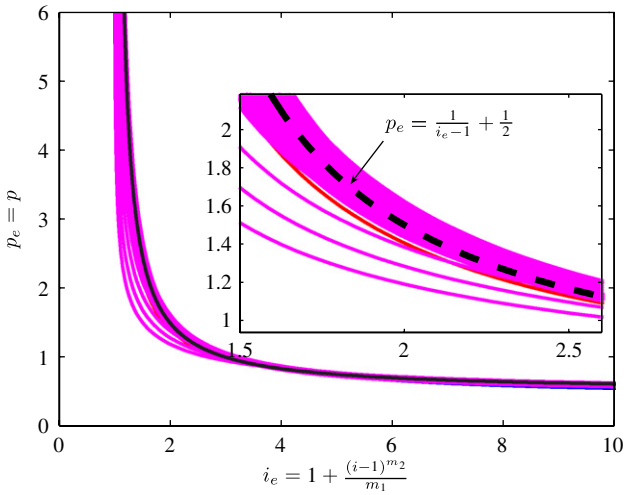

Fig. 27. Unique p_e–i_e diagram, compared with charts of load profiles given by $\lambda = 0.05, 1.05, \ldots, 1$, $\gamma = 0.001, 1.001, 2.001, 3.001$; $d = 1$.

With the values in Table 4 and from Eqs. (41) and (42) we can represent the isodamage curves in the p_e–i_e space for different pulse shapes, in order to compare them with the hyperbole described from Eq. (43). The charts in Fig. 27, related to 82 different pulse shapes, show a maximum discrepancy of 0.488 (24.05%), corresponding to the abscissa $i_e = 1.24$ and a Q value of about 2.49. Therefore, the isodamage curves in p_e–i_e space do not collapse into an unique hyperbolic curve.

4. Conclusions

A parametric analysis of the response spectrum for a sdof system under pulse loads given by high explosives is proposed. It shows a way to establish the structural response by varying the pulse load parameters. However, many properties of the envelope function still have to be demonstrated, as for example the localization of the transition point. The response curve expression used allows to obtain low residuals for the fitted curve, whose input data are generated by computer experiments. The notable complexity of such an expression suggests to investigate simplified analytical forms for isodamage curves. Simple hyperbolic functions seem suitable to fit the data of these diagrams. However, for some load shapes, curves with

sufficiently low values of residuals cannot be obtained when only two parameters m_1 and m_2 are used. Another possibility could be to use a linear combination of hyperbolic function powers, as it was done for the transient response spectrum. Lower values of the sum of squared deviations could allow the isodamage curves to collapse into an unique chart in the effective space, for any value of λ and γ. However, some problems related to the choices of the spectrum domain and the right set of constants $n_0, n_1, \ldots, n_4$ need to be solved, because these solutions have an influence on all the results related to a rigorous dynamic analysis.

Acknowledgments

The research theme is one of the subjects of the Centre of Study and Research for the Identification of Materials and Structures (CIMEST)—"M. Capurso" of the University of Bologna.

References

[1] W.E. Baker, P.A. Cox, P.S. Westine, J.J. Kulesz, R.A. Strehlow, *Explosion Hazards and Evaluation*, Elsevier, London, 1983.
[2] Q.M. Li, H. Meng, Pressure–impulse diagram for blast loads based on dimensional analysis and single-degree-of-freedom model, *Journal of Engineering Mechanics* 128 (1) (2002) 87–92.
[3] Q.M. Li, H. Meng, Pulse loading shape effects on pressure–impulse diagram of an elastic–plastic, single-degree-of-freedom structural model, *International Journal of Mechanical Sciences* 44 (2002) 1985–1998.
[4] T.P. Chang, Dynamic response of space structures under random excitation, *Computers and Structures* 48 (4) (1993) 575–582.
[5] G.K. Schleyer, S.S. Hsu, A modelling scheme for predicting the response of elastic–plastic structures to pulse pressure loading, *International Journal of Impact Engineering* 24 (2000) 759–777.
[6] M.Y.H. Bangash, *Impact and Explosion—Analysis and Design*, Blackwell Scientific Publication, Oxford, 1993.
[7] G.C. Mays, P.D. Smith, *Blast Effects on Buildings—Design of Buildings to Optimize Resistance to Blast Loading*, Thomas Telford, London, 1995.
[8] T. Krauthammer, Blast mitigation technologies: developments and numerical considerations for behaviour assessment and design, *Proceedings of the International Conference on Structures Under Shock and Impact, SUSI*, Computational Mechanics Inc., 1998, pp. 3–12.
[9] G.R. Abrahamson, H.E. Lindberg, Peak load–impulse characterization of critical pulse loads in structural dynamics, *Nuclear Engineering and Design* 37 (1976) 35–46.
[10] J.M. Biggs, *Introduction to Structural Dynamics*, McGraw-Hill, New York, 1964.
[11] C.K. Youngdahl, Correlation parameters for eliminating the effect of pulse shape on dynamic plastic deformation, *ASME Journal of Applied Mechanics* 37 (1970) 744–752.
[12] C.K. Youngdahl, Dynamic plastic deformation of circular cylindrical shells, *ASME Journal of Applied Mechanics* 39 (1972) 746–750.
[13] C.K. Youngdahl, The interaction between pulse shape and strain hardening in dynamic plastic response, *International Journal of Impact Engineering* 7 (1988) 55–70.
[14] G. Zhu, Y.G. Huang, T.X. Yu, R. Wang, Estimation of the plastic structural response under impact, *International Journal of Impact Engineering* 4 (4) (1986) 271–282.
[15] Q.M. Li, N. Jones, Blast loading of fully clamped circular plates with transverse shear effects, *International Journal of Solids and Structures* 31 (14) (1994) 1861–1876.
[16] Q.M. Li, N. Jones, Blast loading of a 'short' cylindrical shell with transverse shear effects, *International Journal of Impact Engineering* 16 (2) (1995) 331–353.
[17] Q.M. Li, N. Jones, Blast loading of fully clamped beams with transverse shear effects, *Mechanics of Structures and Machines* 23 (1) (1995) 59–86.
[18] P.S. Symonds, T.X. Yu, Counterintuitive behavior in a problem of elastic–plastic beam dynamics, *ASME Journal of Applied Mechanics* 52 (1985) 517–522.
[19] Q.M. Li, Y.M. Liu, Uncertain dynamic response of a deterministic elastic–plastic beam, *International Journal of Impact Engineering* 28 (2003) 643–651.
[20] P.D. Smith, J.G. Hetherington, *Blast and Ballistic Loading of Structures*, Butterworth-Heinemann Ltd., London, 1994.
[21] Eurocode 1, Basis of design and actions on structures—part 2–7: actions on structures—accidental actions due to impact and explosions, *UNI ENV 1991-2-7*, September 2000.
[22] H.J. Hansen, A. Kristensen, L. Damkilde, U. Thygesen, Structural analysis of offshore structures exposed to blast loads, *NSCM 15–15th Nordic Seminar on Computational Mechanics*, 2002, pp. 237–240.
[23] B.W. Lindgren, *Statistical Theory*, Macmillan, New York, 1976.
[24] J.R. Florek, H. Benaroya, Pulse-pressure loading effects on aviation and general engineering structures—review, *Journal of Sound and Vibration* 284 (2005) 421–453.